BIOCHEMISTRY
including biophysical chemistry & molecular biology

Article

pubs.acs.org/biochemistry

Proton Uptake and pK_a Changes in the Uncoupled Asn139Cys Variant of Cytochrome *c* Oxidase

Ann-Louise Johansson,[†] Jens Carlsson,[†] Martin Högbom,[†] Jonathan P. Hosler,[‡] Robert B. Gennis,[§] and Peter Brzezinski*,[†]

[†]Department of Biochemistry and Biophysics, The Arrhenius Laboratories for Natural Sciences, Stockholm University, SE-106 91 Stockholm, Sweden

[‡]Department of Biochemistry, University of Mississippi Medical Center, 2500 North State Street, Jackson, Mississippi 39216, United States

[§]Department of Biochemistry, University of Illinois at Urbana-Champaign, Urbana, Illinois 61801, United States

ABSTRACT: Cytochrome *c* oxidase (CytcO) is a membrane-bound enzyme that links electron transfer from cytochrome *c* to O_2 to proton pumping across the membrane. Protons are transferred through specific pathways that connect the protein surface with the catalytic site as well as the proton input with the proton output sides. Results from earlier studies have shown that one site within the so-called D proton pathway, Asn139, located ∼10 Å from the protein surface, is particularly sensitive to mutations that uncouple the O_2 reduction reaction from the proton pumping activity. For example, none of the Asn139Asp (charged) or Asn139Thr (neutral) mutant CytcOs pump protons, although the proton-uptake rates are unaffected. Here, we have investigated the Asn139Cys and Asn139Cys/Asp132Asn mutant CytcOs. In contrast to other structural variants investigated to date, the Cys side chain may be either neutral or negatively charged in the experimentally accessible pH range. The data show that the Asn139Cys and Asn139Asp mutations result in the same changes of the kinetic and thermodynamic parameters associated with the proton transfer. The similarity is not due to introduction of charge at position 139, but rather introduction of a protonatable group that modulates the proton connectivity around this position. These results illuminate the mechanism by which CytcO couples electron transfer to proton pumping.

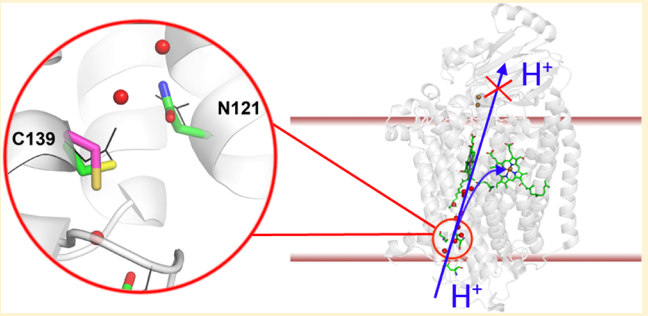

The aa_3-type cytochrome *c* oxidase (CytcO) belongs to a superfamily of membrane-bound enzyme complexes that catalyze the reduction of molecular oxygen to water in aerobic organisms. Most members of this family couple the oxygen reduction reaction to proton pumping across the membrane, thereby contributing to the maintenance of an electrochemical proton gradient (for reviews on the structure and function of CytcOs, see, e.g., refs 1−9). The CytcO from *Rhodobacter sphaeroides* receives electrons from a water-soluble cytochrome *c*, which binds on the more positive (*p*) side of the membrane. Initially, the primary acceptor Cu_A is reduced, which is followed in time by the transfer of an electron to a heme group (heme *a*) and the catalytic site, composed of another heme group (heme a_3) and a copper site (Cu_B). The protons needed for oxygen reduction are transferred to the catalytic site from the more negative (*n*) side of the membrane, via two proton pathways (denoted D and K), which consist of water molecules and protonatable amino acid residues. The D pathway, which is the focus of this paper, is also used for the transfer of protons that are translocated (pumped) from the *n* to *p* side of the membrane. This pathway starts at an aspartate residue (Asp132),[a] near the *n* side surface, and ends at a glutamate residue (Glu286) ∼25 Å from Asp132, between the heme cofactors (Figure 1a).[10,11] Glu286 is an internal proton donor[12,13] and the branching point from which protons are transferred either to the catalytic site or toward a "pump site" from where they are translocated to the *p* side of the membrane. It is also likely that the Glu286 side chain may adopt different orientations and that changes between these different positions modulate proton-transfer rates to the catalytic site and the pump site, respectively.[14−24] In other words, the Glu286 residue is an important functional component of the CytcO. The structural components involved in gating of the pumped protons are most likely located at a different site.[25]

Proton-transfer reactions through the D pathway can be studied by monitoring the kinetics of specific reaction steps during the reaction of the reduced CytcO with O_2. In this experiment, the CytcO is reduced by four electrons when one electron is added to each of the four redox sites, Cu_A, heme *a*, heme a_3, and Cu_B. The reduced CytcO is incubated under an atmosphere of carbon monoxide, which leads to binding of the

Received: November 28, 2012
Revised: January 9, 2013
Published: January 10, 2013

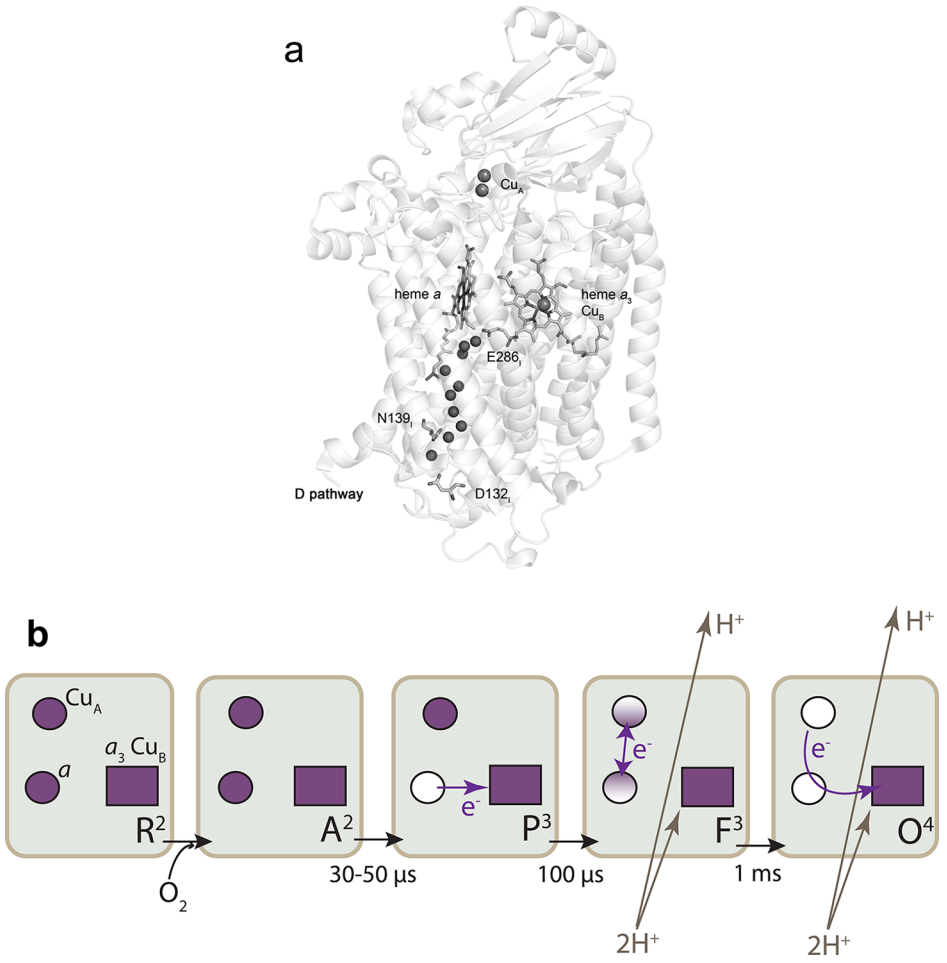

Figure 1. (a) Structure of cytochrome *c* oxidase from *R. sphaeroides* (PDB entry 1M56). The four redox cofactors are Cu_A, heme *a*, and catalytic site consisting of heme a_3 and Cu_B. The electron donor, cytochrome *c* (not shown), binds at the surface near the Cu_A site. The D proton pathway starts at Asp132, near the CytcO surface, and leads via Asn139 and ~10 water molecules to Glu286. The other, K proton pathway is not shown. This figure was prepared using MacPymol.[67] (b) Schematic illustration of the reaction studied in this work. The redox-active cofactors Cu_A and heme *a* are shown as circles, and the heme a_3–Cu_B catalytic site is shown as a square. The filled and empty symbols represent reduced and oxidized sites, respectively. The reaction is initiated from a state in which all four redox sites are reduced ($\mathbf{R}^2$, where the superscript indicates the number of electrons at the catalytic site). When O_2 binds to heme a_3, state $\mathbf{A}^2$ is formed. It is followed in time by the transfer of an electron from heme *a* to the catalytic site forming state $\mathbf{P}^3$ with a time constant of 30–50 μs. The $\mathbf{P}^3 \rightarrow \mathbf{F}^3$ reaction with a time constant of ~100 μs (at pH <9) does not involve the further electron transfer to the catalytic site, but it is linked in time to the uptake of a proton to the catalytic site, proton pumping, and fractional electron transfer from Cu_A to heme *a* (indicated as half-filled circles). Finally, during the $\mathbf{F}^3 \rightarrow \mathbf{O}^4$ reaction, the electron from the Cu_A–heme *a* equilibrium is transferred to the catalytic site (with a time constant of ~1 ms at pH 7), accompanied by the uptake of a proton to the catalytic site and proton pumping across the membrane.

CO ligand to the reduced heme a_3. The reduced CytcO–CO complex is mixed with an O_2-saturated solution, after which the blocking CO ligand is removed by means of a short laser flash (this technique and recent results from studies using this approach are described, for example, in reviews 8, 26, and 27). We denote the reduced state of the CytcO as $\mathbf{R}^2$, where the superscript signifies the number of electrons at the catalytic site (when the enzyme is fully reduced, there are two additional electrons at heme *a* and Cu_A). After O_2 binds to heme a_3, an electron is transferred from heme *a* to the catalytic site, which is associated with breaking of the O–O bond and the formation of state $\mathbf{P}^3$ with a time constant of 30–50 μs (Figure 1b). Over this time scale, the transfer of the electron leaves the catalytic site with an excess negative charge. Consequently, formation of the $\mathbf{P}^3$ reaction intermediate is followed in time by proton uptake, through the D pathway, to the catalytic site with a time constant of ~100 μs (at pH 7.5), resulting in the formation of the $\mathbf{F}^3$ state. The $\mathbf{P}^3 \rightarrow \mathbf{F}^3$ reaction is also associated with the pumping of protons across the membrane. The proton transfer during the $\mathbf{P}^3 \rightarrow \mathbf{F}^3$ reaction displays pH-dependent kinetics, where in a detergent solution the rate is proportional to the protonation state of a residue with a pK_a of 9.4, previously attributed to Glu286[12,13,28] (see also ref 29). In the final step of the reaction, the fourth electron is transferred to the catalytic site, linked to proton uptake through the D pathway, forming the oxidized CytcO, and proton pumping with a time constant of ~1 ms (at pH 7). Also, this reaction displays pH-dependent kinetics. However, the pH dependence profile is more complex as the reaction involves a coupled electron–proton transfer and presumably both processes display pH-dependent kinetics. Two pK_a values are observed, where one of these pK_a values, <6.3, was attributed to titration of a group that interacts with the heme groups (the protonation state affects the electron-transfer rate to the catalytic site), while the other pK_a of ~9 was attributed to Glu286 (cf. proton transfer equivalent to that during the $\mathbf{P}^3 \rightarrow \mathbf{F}^3$ reaction).[4]

dx.doi.org/10.1021/bi301597a | *Biochemistry* 2013, 52, 827–836

Data from earlier studies have shown that mutation of Asp132 to its nonprotonatable analogue, Asn (Asp132Asn mutant CytcO), resulted in slowing the proton-uptake kinetics through the D pathway by a factor of ~5000 to 2 s^{-1} (τ = 0.5 s).[12,30] Even though with the Asp132Asn mutant CytcO, no proton uptake over the time scale of the $\mathbf{P}^3 \rightarrow \mathbf{F}^3$ reaction is observed, the $\mathbf{F}^3$ state is formed with a time constant of ~100 μs because the proton required for $\mathbf{F}^3$ formation is transferred internally from Glu286,[12] which is then left in the transiently unprotonated state in the time range of ~100 μs to 0.5 s.[13,30] Replacement of Asn139, further up the D pathway (see Figure 1a), with several different amino acid residues resulted in uncoupling of proton pumping from O_2 reduction.[31−33] In some cases, such as for the Asn139Asp and Asn139Thr mutations, the maximal rate of uptake of protons via the D pathway was not affected and the maximal O_2 reduction rate was the same as with wild-type CytcO.[27,34,35] The uncoupling of proton pumping from O_2 reduction was suggested to be related to a pK_a shift of Glu286, which was >1.6 and −1.8 units for the Asn139Asp[34] and Asn139Thr[35] mutant CytcOs, respectively. Analysis of the pH dependence of the proton-transfer kinetics through the D pathway in these mutant CytcOs, as well as in many other structural variants in which D pathway residues were modified, allowed for detailed theoretical analyses of proton-transfer mechanisms and proton gating in CytcO,[21,24,36−40] yet a detailed molecular explanation for a link between structural alterations ~20 Å from the proton gating region (around Glu286) and complete elimination of the pumping activity is still lacking.

In this study we have investigated the transfer of protons through the D pathway in the Asn139Cys structural variant, which does not pump protons.[33,41] This mutant CytcO was engineered and studied to answer the functional questions mentioned above. As for the Thr, the Cys side chain is essentially uncharged at neutral pH in water. However, the Cys side chain may lose its proton in the experimentally accessible pH range, yielding a negatively charged site, i.e., a situation similar to that with the Asn139Asp mutant CytcO, but with a pK_a difference of ~4 units between the Cys (~8) and Asp (~4) side chains. A comparison of the kinetic and thermodynamic parameters for the different Asn139X (X = Asp, Thr, or Cys) mutants shows that the behavior of the Asn139Cys mutant CytcO is similar to that of Asn139Asp. The similarity is presumably not due to the introduction of charge at position 139, but rather a protonatable group.

MATERIALS AND METHODS

Expression and Purification. The expression of the CytcO structural variants was performed as previously described.[42,43] Purification of the His-tagged CytcO variants was performed using immobilized metal ion affinity chromatography (IMAC) on a Ni-NTA resin (Qiagen), as previously described.[43] After purification, the solution for the enzyme was exchanged for buffer containing 100 mM HEPES (pH 7.5) and 0.05% DDM (*n*-dodecyl β-maltoside). The enzyme was rapidly frozen in liquid N_2 and stored in −80 °C until it was used.

Preparation of Fully Reduced and CO-Bound CytcO for Flow-Flash Measurements. For measurements of the pH dependence, the enzyme buffer was exchanged for 1 mM HEPES (pH 7.5) and 0.05% DDM by concentration and redilution using filter tubes with a 100 kDa cutoff (Amicon Ultra, Millipore). Finally, the CytcO was diluted to a final concentration of 10 μM. For control experiments at pH 7.5 and 10.0, the enzyme was kept in buffers containing 100 mM HEPES (pH 7.5) or exchanged for 100 mM CAPS (pH 10.0) (0.05% DDM). The enzyme solution was transferred to an anaerobic cuvette, and the air in the cuvette was exchanged for N_2. To reduce the enzyme, ascorbate and hexaammineruthenium chloride were added (final concentrations of 2 mM and 1 μM, respectively) to the anaerobic CytcO solution. The redox state of the enzyme was checked using UV−vis spectroscopy, and upon full reduction, the N_2 atmosphere was replaced with CO. The formation of the fully reduced CO complex was verified from the absorption spectrum.

Flow-Flash Measurements. The fully reduced CO-bound enzyme was rapidly mixed at a 1:5 ratio with oxygen-saturated buffer in a stopped-flow apparatus (Applied Photophysics). The O_2 buffer contained 100 mM MES [2-(*N*-morpholino)-ethanesulfonic acid] (pH 6.0−6.5), 100 mM HEPES [4-(2-hydroxyethyl)-1-piperazineethanesulfonic acid] (pH 7.0−7.5 or 8.0), 100 mM Tris (pH 8.5), 100 mM CHES [2-(*N*-cyclohexylamino)ethanesulfonic acid] (pH 9.0−9.5), or 100 mM CAPS (*N*-cyclohexyl-3-aminopropanesulfonic acid) (pH 10.0−10.5) and 0.05% DDM. Approximately 200 ms after the samples had been mixed a short laser flash (Quantel Brilliant Nd:YAG laser, 532 nm) was used to dissociate the CytcO−CO complex to allow oxygen to bind to the catalytic site. The reaction between CytcO and oxygen was then monitored at specific wavelengths with a time resolution of ~100 ns. Kinetic data analysis was performed using Pro-K (Applied Photophysics).

Preparations of CytcO for Proton-Uptake Measurements. The buffer for the enzyme solution was exchanged for a solution containing 100 mM KCl (pH 7.8) and 0.05% DDM. The pH-sensitive dye phenol red was added to a final concentration of 40 μM, and the enzyme solution was transferred to an anaerobic cuvette. After that, the sample preparation was as described above for the flow-flash measurements, and the experiments were performed as described above. Absorbance changes of the pH dye, associated with proton uptake, were monitored at 560 nm.

Molecular Dynamics (MD) Simulations. The MD simulations of CytcO were conducted in two steps. In the first step, the structure of CytcO (PDB entry 1m56[11]) was inserted into a hydrated POPC bilayer patch oriented in the *x*−*y* plane. Lipid and water molecules that overlapped with protein atoms were deleted, and ions were added to neutralize the system. The resulting system was placed in a triclinic box, which resulted in a system with ~199000 atoms that was simulated using GROMACS version 4.5.3.[44] The protein was modeled with the OPLSAA force field;[45] POPC interactions were described with the Berger force field parameters,[46] and water molecules were described using the TIP3P model.[47] After a short energy minimization, the membrane and water were equilibrated for 10 ns while the protein atoms were restrained to their initial positions (1000 kJ mol^{-1} nm^{-2}).

In the second step, a snapshot of CytcO from the first simulation was used as starting coordinates for unrestrained simulations in a spherical system with a radius of 28 Å centered on Asn139. The unrestrained MD simulations were performed with the Q software package[48] using the OPLS all-atom force field,[45] Berger lipids,[46] and TIP3P waters.[47] The simulations were conducted in a 28 Å sphere centered on Asn139. The atoms of the heme group that were part of the spherical system, i.e., the hydroxyfarnesylethyl group, were parametrized on the basis of the OPLS all-atom force field.[45] The SHAKE

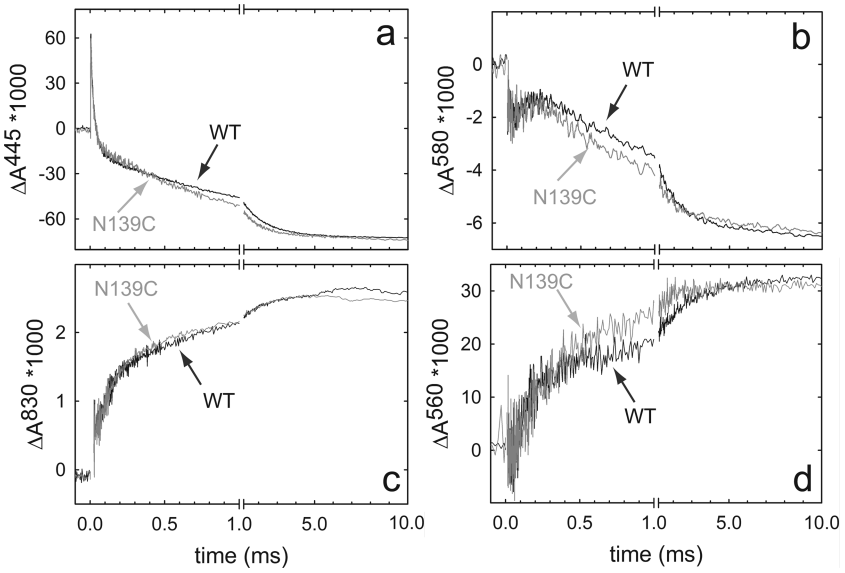

Figure 2. Absorbance changes associated with reaction of the four-electron reduced wild-type and Asn139Cys CytcOs with O_2. (a) Absorbance changes at 445 nm report primarily oxidation of the heme groups heme *a* and a_3. (b) At 580 nm, the initial decrease in absorbance with a time constant of ~50 μs is associated with the transfer of an electron from heme *a* to the catalytic site and formation of the $\mathbf{P}^3$ state. The increase in absorbance with a time constant of ~110 μs is associated with the $\mathbf{P}^3 \rightarrow \mathbf{F}^3$ reaction. The final decrease in absorbance with a time constant of ~1 ms is associated with the $\mathbf{F}^3 \rightarrow \mathbf{O}^4$ reaction. (c) Absorbance changes at 830 nm are primarily associated with oxidation of Cu_A (absorbance increase) during the $\mathbf{P}^3 \rightarrow \mathbf{F}^3$ ($\tau \cong 110$ μs) and $\mathbf{F}^3 \rightarrow \mathbf{O}^4$ ($\tau \cong 1$ ms) transitions. (d) Absorbance changes at 560 nm of the pH-sensitive dye phenol red in the absence of buffer. An increase in absorbance is associated with net proton uptake, which occurs over the same time scales as the $\mathbf{P}^3 \rightarrow \mathbf{F}^3$ and $\mathbf{F}^3 \rightarrow \mathbf{O}^4$ reactions. Experimental conditions: ~2 μM reacting enzyme in 100 mM HEPES (pH 7.5) and 0.05% DDM, $[O_2] \cong 1$ mM, $T = 22$ °C. The traces have been normalized to 1 μM reacting enzyme. For the data in panel d, the buffer was replaced with 100 mM KCl and 40 μM phenol red was added (pH 7.8).

algorithm[49] was applied to all solvent molecules, and waters at the sphere surface were subjected to radial and polarization restraints.[48,50] A nonbonded cutoff of 10 Å was used, and long-range electrostatic interactions were treated with the local reaction field (LRF) multipole expansion method.[51] All atoms outside the simulation sphere were highly restrained to their initial coordinates and excluded from all nonbonded interactions. The time step was set to 1 fs, and nonbonded pair lists were updated every 25 steps. All Asp, Glu, Arg, and Lys residues within 24 Å of the sphere center were set to their charged states, unless noted otherwise. All other ionizable residues in the system were set to their neutral state. The protonation states for the His residues were set by manual inspection of the structure around the side chain. In the D pathway, Glu286 was protonated and His26 and Asp132 were both ionized in all simulations. In the simulation of the Asn139Cys mutant CytcO, the Cys139 residue was protonated. The mutant structures Asn139Cys and Asn139Cys/Asp132Asn were prepared manually on the basis of the wild-type structure. Each system (wild type, Asn139Cys, and Asn139Cys/Asp132Asn) was first equilibrated by being slowly heated to 300 K while strong restraints on the solute atoms to their initial coordinates were gradually released, and this was followed by a 2−6 ns unrestrained simulation.

pK_a Calculations. Calculations of equilibrium pK_a values in the D pathway were based on the CytcO crystal structure (PDB entry 1m56)[11] and 20 MD simulation snapshots. The calculations were conducted for the wild type, Asn139Cys, and Asn139Cys/Asp132Asn. Calculations of pK_a values were conducted using both the PROPKA[52] and multiconformation continuum electrostatic (MCCE)[53] methods. PROPKA is an empirical structure-based method for predicting pK_a values of ionizable residues, and PROPKA version 3.1, which includes the effect of ligands and cofactors, was used in the calculations. The MCCE method is based on continuum electrostatics calculations and allows a residue to have multiple conformational states and includes optimization of hydrogen bonds. Default settings, where the protein and solvent dielectric constants were set to 4 and 80, respectively, were used in all calculations, and side chain sampling was conducted in 120° increments. The continuum electrostatics calculations were conducted in Delphi.[54] All amino acids within 4 Å of Asp132, Asn139, and Glu286 were defined as "hot spots", which increased the level of conformational sampling in the residues in the D pathway. The heme group was represented by parameters available in MCCE version 2.4. All solvent molecules were removed from the MD snapshots, and the POPC lipid atoms were treated as neutral. For the crystal structures, a 30 Å slab of neutral atoms was added in the MCCE calculation, but no membrane was present in the PROPKA calculations.

RESULTS

The overall oxygen-reduction activities of the Asn139Cys and Asn139Cys/Asp132Asn CytcOs have previously been determined to be at least ~90% and 12−15%, respectively, of that found with the wild-type *R. sphaeroides* CytcO.[33,55] In the Asn139Cys structural variant, oxygen reduction was uncoupled from proton pumping (the proton pumping stoichiometry was <5% of that of the wild-type CytcO).[33] The Asn131Cys mutation in the *Paracoccus denitrificans* CytcO (corresponds to the Asn139Cys mutation in the *R. sphaeroides* CytcO) also resulted in impaired proton pumping, and the activity was ~86% of that of the wild-type CytcO.[41]

dx.doi.org/10.1021/bi301597a | *Biochemistry* 2013, 52, 827−836

Electron- and proton-transfer reactions associated with oxidation of the reduced Cyt*c*O were monitored by measuring absorbance changes at specific wavelengths after flash-induced dissociation of the CO ligand from heme a_3. We focus on the $\mathbf{P}^3 \rightarrow \mathbf{F}^3$ and $\mathbf{F}^3 \rightarrow \mathbf{O}^4$ reactions because in the wild-type Cyt*c*O these reactions are linked to the uptake of protons from solution and proton pumping.

Reaction of the Reduced Cyt*c*O with O_2. At 445 nm (Figure 2a), oxygen binding ($\tau \cong 8$ μs at 1 mM O_2) and the oxidation of the heme groups ($\tau \cong 1$ ms) are both seen as a decrease in absorbance. The $\mathbf{P}^3 \rightarrow \mathbf{F}^3$ and $\mathbf{F}^3 \rightarrow \mathbf{O}^4$ reactions are observed at 580 nm (Figure 2b). Here, the rapid, small decrease in absorbance after the laser flash at time zero is associated with the transfer of an electron from heme *a* to the catalytic site and formation of state $\mathbf{P}^3$ with a time constant of ~50 μs. The increase in absorbance with a time constant of ~110 μs ($k = 8900 \pm 800$ s^{-1}) is in part due to formation of the $\mathbf{F}^3$ state, which is associated with the transfer of a proton to the catalytic site. This increase in absorbance also contains a contribution from fractional electron transfer from Cu_A to heme *a* (i.e., reduction of heme *a*). Oxidation of Cu_A in this reaction is seen as an increase in absorbance at 830 nm (Figure 2c) (~50% oxidation of the copper site with a time constant of ~100 μs). The subsequent absorbance decrease at 580 nm and increase at 830 nm are associated with the transfer of an electron from the Cu_A–heme *a* equilibrium, linked to proton transfer, to the catalytic site, forming the oxidized Cyt*c*O (state $\mathbf{O}^4$) with a time constant of ~1.2 ms ($k = 860 \pm 30$ s^{-1}).

With the Asn139Cys mutant Cyt*c*O, the time constant of the $\mathbf{P}^3 \rightarrow \mathbf{F}^3$ reaction was ~130 μs ($k = 7550 \pm 740$ s^{-1}) at pH 7.5 (Figure 2a), i.e., approximately the same as that for the wild-type Cyt*c*O. The $\mathbf{F}^3 \rightarrow \mathbf{O}^4$ reaction was slightly faster with the mutant than with the wild-type Cyt*c*O; at pH 7.5, we observed a time constant of ~770 μs ($k = 1300 \pm 53$ s^{-1}).

Proton uptake during the oxidation reaction (through the D pathway) was investigated by measuring absorbance changes of the pH-sensitive dye phenol red at 560 nm. For the Asn139Cys Cyt*c*O variant, two proton-uptake phases were observed (Figure 2d). The first phase displayed a time constant of ~100 μs (53% of the total amplitude), while the second phase displayed a time constant of ~700 μs (47% of the total amplitude). Thus, as with the wild-type Cyt*c*O, these two components overlapped in time with the $\mathbf{P}^3 \rightarrow \mathbf{F}^3$ and $\mathbf{F}^3 \rightarrow \mathbf{O}^4$ reactions, respectively.

The pH dependencies of the kinetics of the $\mathbf{P}^3 \rightarrow \mathbf{F}^3$ and $\mathbf{F}^3 \rightarrow \mathbf{O}^4$ reactions were studied by allowing the reduced Cyt*c*O to react with O_2 at different pH values in the range of 6–10.5. As already mentioned above and seen in Figure 3a, the $\mathbf{P}^3 \rightarrow \mathbf{F}^3$ reaction rate with the wild-type Cyt*c*O displays a titration curve with an apparent pK_a of 9.4.[28] With the Asn139Cys mutant Cyt*c*O, the reaction rate was essentially pH-independent (on average ~1×10^4 s^{-1}; $\tau \cong 100$ μs) in the measured pH range, with only a slight decrease at the highest pH value of 10.5. Thus, the apparent pK_a in the pH dependence was shifted from 9.4 to higher values (see Discussion). Similarly, the rate of the $\mathbf{F}^3 \rightarrow \mathbf{O}^4$ reaction in the Asn139Cys variant (Figure 3b) was only weakly pH-dependent, displaying on average rates higher than those observed with the wild-type Cyt*c*O.

For the Asn139Cys/Asp132Asn structural variant, after the absorbance changes associated with O_2 binding and formation of state $\mathbf{P}^3$, the oxidation time constant was ~330 ms at pH 7.5 (Figure 4a), i.e., a factor of ~300 or ~400 slower than that observed with the wild-type or Asn139Cys mutant Cyt*c*O,

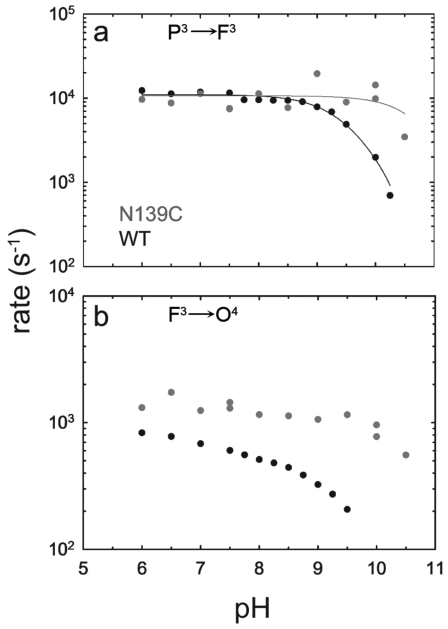

Figure 3. pH dependence of the $\mathbf{P}^3 \rightarrow \mathbf{F}^3$ (a) and $\mathbf{F}^3 \rightarrow \mathbf{O}^4$ (b) reactions in the wild-type and Asn139Cys Cyt*c*Os. The rates were extracted from measurements at 445 and 580 nm. Experimental conditions: 1–2 μM reacting enzyme, 100 mM MES, HEPES, Tris-HCl, CHES, or CAPS, depending on the pH, 0.05% DDM, $[O_2] \cong 1$ mM, $T = 22$ °C.

respectively (1.2 ms or 770 μs, respectively). In contrast to the results obtained with the Asp132Asn mutant Cyt*c*O, with the Asn139Cys/Asp132Asn structural variant we observed a fractional rapid proton uptake with a time constant of ~250 μs and an amplitude of ~30% of that observed with the wild-type Cyt*c*O. The maximal pH dye absorbance change was reached with a time constant that was the same as that of $\mathbf{O}^4$ formation (i.e., 330 ms) with the Asn139Cys/Asp132Asn Cyt*c*O (not shown). The Cu_A site [absorbance changes at 830 nm (Figure 4c)] was oxidized by ~40% with a time constant of ~250 μs, while the remaining part was oxidized with a time constant of ~330 ms. The 250 μs fractional proton uptake and the accompanying oxidation of Cu_A would indicate that the $\mathbf{F}^3$ state is formed with this time constant in 30–40% of the Cyt*c*O population. A small increase in absorbance was observed at 580 nm (Figure 4b). However, it was difficult to determine the time constant of this absorbance change as it was smaller than that observed with the wild-type Cyt*c*O (on the basis of the data described above for the proton uptake and Cu_A oxidation, we would expect to see 30–40% of the 580 nm absorbance change) and partly masked by a decrease in absorbance associated with the formation of the $\mathbf{P}^3$ state.

Theoretical Calculations. Two theoretical approaches were used to estimate the protonation states of Cys139 in the Asn139Cys and Asn139Cys/Asp132Asn mutant Cyt*c*Os and the potential effects of these mutations on the Glu286 pK_a. Results from both experimental and theoretical studies indicate that the pK_a value of Glu286 in the wild-type Cyt*c*O is elevated by several units compared to the solution value,[20,21,56−58] which is also confirmed by the calculations in this study for the wild type and the two mutant Cyt*c*Os (see Table 1). The use of the PROPKA method predicted a Glu286 pK_a value of ~9 for both the crystal structure and the MD snapshots, whereas the MCCE method predicted a fully protonated side chain over the

dx.doi.org/10.1021/bi301597a | *Biochemistry* 2013, 52, 827–836

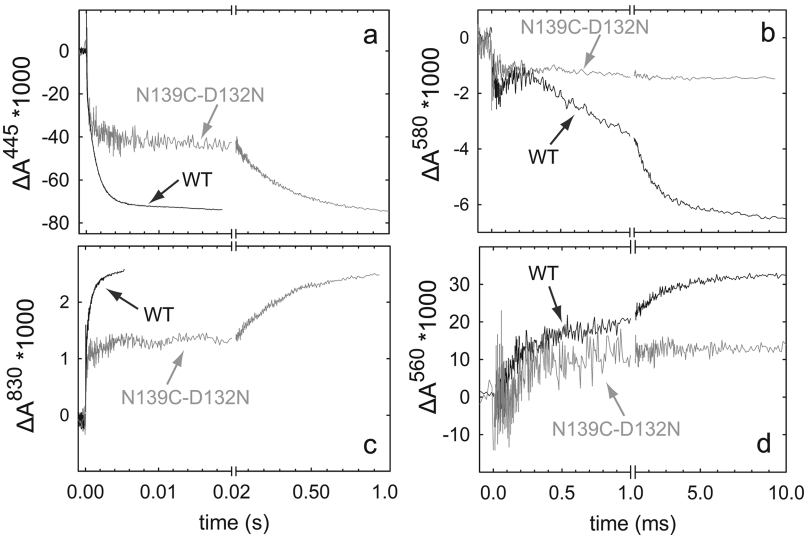

Figure 4. Absorbance changes associated with reaction of the four-electron reduced wild-type and Asn139Cys/Asp132Asn CytcOs with O_2. See Figure 2 for a description of the reactions at the different wavelengths and experimental conditions.

Table 1. pK_a Values Calculated from the Crystal Structure and Molecular Dynamics Snapshots Using the PROPKA and MCCE Methods

		MCCE		PROPKA	
mutant	amino acid	X-ray structures[a]	MD snapshots[b]	X-ray structures[a]	MD snapshots[b]
WT	E268	>14	>14	8.8	8.7
N139C	C139	>14	>13	12.8	13.0
	E268	>14	>14	8.8	9.0
N139C/D132N	C139	>14	>14	12.2	12.4
	E268	>14	>14	8.8	9.1

[a]Average over chain A and chain B of the crystal structure. [b]Calculated as an average over 20 snapshots from an MD simulation.

titrated pH range (pK_a > 14). The Cys in the Asn139Cys mutant CytcO also had a pK_a value elevated by ~4 units in the PROPKA calculation, and values of >13 were obtained using the MCCE method.

The conformations of amino acid residues in the protein segment around position 139 were analyzed on the basis of MD simulations, and representative snapshots are shown in Figure 5. As seen in Figure 5B, the Asn121 side chain moves down toward Asn139 and a water molecule, found in the X-ray crystal structure, is displaced. Upon replacement of Asn139 with Cys in the Asn139Cys and Asn139Cys/Asp132Asn mutants, the Asn121 side chain samples both the crystal structure conformation and the one observed in the MD simulation of wild-type CytcO. The side chain of Cys139 in these two mutants also explored two main conformations, in which the SG atom pointed either into the D pathway or toward residue 132 (Figure 5).

DISCUSSION

In this work, we have studied reactions linked to the transfer of a proton through the D pathway of CytcO during O_2 reduction. As discussed above, results from earlier studies have shown that the $\mathbf{P}^3 \rightarrow \mathbf{F}^3$ reaction rate displays a pH dependence that could be described by a Henderson−Hasselbalch equation with a pK_a of 9.4.[28] We have previously attributed this pK_a to Glu286 (but see more detailed discussion below). The model holds that there is a rapid (>10^4 s^{-1}) proton equilibrium between solution and Glu286, and the rate of transfer of a proton from Glu286 to the catalytic site is 1×10^4 s^{-1}. Consequently, when pH < pK_a, Glu286 is fully protonated and the observed proton-uptake rate constant is 1×10^4 s^{-1}. When pH > pK_a, the fraction of protonated Glu286 decreases with increasing pH, and therefore, the observed rate also decreases (see also ref 29 for an alternative explanation of our data). This scenario is described by the following equation, where k_{PF} is the observed $\mathbf{P}^3 \rightarrow \mathbf{F}^3$ rate, pK_a is that of Glu286, and k_H is the rate of transfer of a proton from Glu286 to the catalytic site (10^4 s^{-1}):

$$k_{PF} = \frac{k_H}{1 + 10^{pH-pK_a}}$$

If the pK_a of Glu286 would increase as a result of a mutation (as observed for the Asn139Cys mutant CytcO), according to this model the observed rate at high pH would increase. Such an increase would be observed without any changes to the rates of transfer of protons from solution to Glu286 or from Glu286 to the catalytic site. This description is, of course, simplified in part because the pK_a is determined from the pH dependence of the kinetics of a proton-transfer reaction (during the $\mathbf{P}^3 \rightarrow \mathbf{F}^3$ reaction step) and not a direct titration of the residue. Consequently, the observed pK_a must not necessarily be the true pK_a of the residue. Because Glu286 can adopt different orientations[14,15,17,23] and the transfer of a proton from the Glu residue may take place only in one of these conformations, the measured pK_a value may also involve the free energy contribution from reorientation of the Glu286 side chain upon proton transfer (refs 21, 27, and 36 and also 59). Here, we call this pK_a value p$K_{a,PF}$ to emphasize the fact that it is determined from studies of a specific reaction. As already discussed above, results from earlier studies have shown that the p$K_{a,PF}$ value could be shifted up or down upon mutation of residues within the D pathway, for example, at position Asn139. These pK_a shifts were suggested to be linked to changes in the proton pumping stoichiometry[21,27] because they would modulate the relative rate of transfer of protons to the pump and catalytic sites.

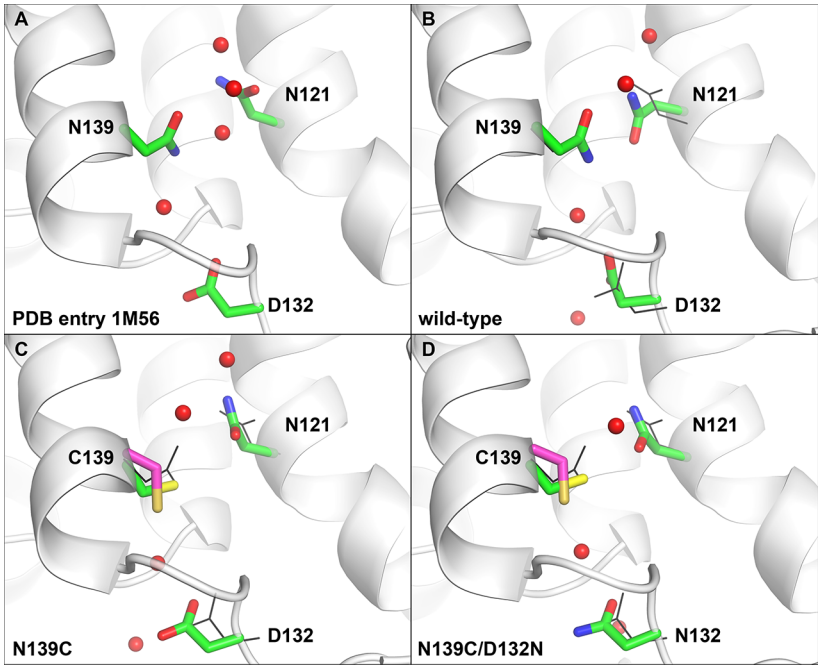

Figure 5. Crystal structure of Cyt*c*O (A, PDB entry 1m56) and representative snapshots from molecular dynamics simulations of the wild type (B), Asn139Cys (C), and Asn139Cys/Asp132Asn (D). Cyt*c*O is displayed as a cartoon, and selected amino acid residues in the D pathway are shown as sticks. In panels c and d, two different configurations of the Cys139 side chain are shown (see the text). In panels B and C, the amino acid side chain conformations for Asn121, Asn139, and Asp132 in the crystal structure are shown as black lines.

Results from experimental and theoretical studies indicate that the Asn139 site is important for controlling the transfer of protons through the D pathway, and structural changes at this site possibly also affect proton transfer further up the pathway. For example, calculations on the crystal structure of the oxidized Cyt*c*O from *R. sphaeroides* indicate that the D pathway is in a closed state at Asn139.[40] This result is consistent with our MD simulations (Figure 5B), although with a different configuration of Asn139. Transient changes in the Asn139 side chain conformation result in opening of the pathway.[40] These structural changes may also be linked to changes around Glu286 as evidenced from FTIR experiments,[32] which indicate that there is a structural link between these two sites. This conclusion is also supported by an analysis of the structure of the Asn139Asp mutant Cyt*c*O from *P. denitrificans*.[41]

In the Asn139Cys mutant Cyt*c*O studied here, the value of $pK_{a,PF}$ increased to >11, and it has been observed previously[33] that the mutant Cyt*c*O does not pump protons. When discussing the reason for this uncoupling, we think it is relevant to consider whether the Cys side chain is charged. It has been shown that without subunit III the Cys139 residue may be transiently deprotonated during turnover.[55] Results from earlier studies have shown that introduction of a purely structural alteration at the Asn139 site (Asn139Thr mutant Cyt*c*O) results in a relatively large change in the $pK_{a,PF}$; the value decreased by 1.8 units, from 9.4 to 7.6.[35] Introduction of a charged residue also resulted in a large shift in the $pK_{a,PF}$. However, in this case, the $pK_{a,PF}$ instead increased by at least 1.6 units to >11.[34] Also, the question of whether the sign and magnitude of the $pK_{a,PF}$ shift are related to the charge at position 139 arises.

When addressing the charge issue, we start with a discussion of effects of mutations at another, nearby site, Asp132. As mentioned above, replacement of Asp132 with its non-protonatable analogue Asn, resulted in slowing the proton-uptake rate by a factor of 5000 ($\tau \cong 0.5$ s) compared to that of the wild-type Cyt*c*O.[12,13,30,60] Introduction of an aspartate at position 139 in the Asp132Asn mutant Cyt*c*O (Asp132Asn/Asn139Asp double-mutant Cyt*c*O) resulted in acceleration of the steady-state activity as compared to that with the Asp132Asn single-mutant Cyt*c*O[55,61] and acceleration of the proton-uptake rate by a factor of ~17, to ~30 ms.[61] This effect is qualitatively the same as that observed earlier in similar experiments with, for example, the *Escherichia coli* cytochrome bo_3 quinol oxidase[62] and photosynthetic reaction centers.[63] In these systems, slowing in a proton-uptake rate upon removal of a carboxylate near the surface could be partly compensated for by introduction of another carboxylate at nearby locations. This effect was attributed to the removal and reintroduction of negative charge near an entry site of a proton pathway. The same explanation may be offered for the behavior of the Asp132Asn/Asn139Asp double-mutant Cyt*c*O; i.e., removal of negative charge at Asp132 would result in slowing the proton uptake, and addition of a negative charge at Asp139 (in the Asp132Asn/Asn139Asp double mutant) would result in partial restoration of the proton-uptake rate. The restoration is suggested to be only partial because position 139 is farther from the protein surface than position 132, or position 139 may not be fully deprotonated. However, more important than charge compensation may be introduction of an alternative proton acceptor or donor at position 139 when Asp132 is replaced with a nonprotonatable residue.[55] Here, removal of SUIII from the Asp132Asn/Asn139Asp or Asp132Asn/Asn139Cys double-mutant Cyt*c*O was shown to yield Cyt*c*O with steady-state activities similar to that of the wild-type Cyt*c*O (without SUIII). Also with SUIII, a protonatable residue at position 139 would be able to shuttle protons into the D pathway, but with a slower rate due to steric obstruction by SUIII.[55]

dx.doi.org/10.1021/bi301597a | *Biochemistry* 2013, 52, 827−836

In the Asn139Cys/Asp132Asn double mutant studied here, we also observed a fractional ($\sim^1/_3$) rapid proton uptake and electron transfer from Cu_A to heme *a*. Thus, in ~30% of the population, proton uptake was slowed only to a small extent (by a factor of 2.5) compared to that of the wild-type Cyt*c*O, while in the major population of the Cyt*c*O (~70%), proton uptake was dramatically slowed to 330 ms; i.e., the proton-uptake rate was similar to that observed with the Asp132Asn single-mutant Cyt*c*O. Considering only charge−charge interactions and the data described above for the Asp132Asn/Asn139Asp double-mutant Cyt*c*O, this observation would imply that the Cys139 residue in 70% of the Asn139Cys/Asp132Asn double-mutant Cyt*c*O is in the neutral state. If so, then in the Asn139Cys single mutant the Cys139 residue would be primarily in the uncharged state at neutral pH because here Asp132 presumably carries a negative charge [refs 58, 59, and 64 and Table 1 (results with the X-ray crystal structure)], which would further stabilize the protonated state of the Cys139 residue (compared to the Asn139Cys/Asp132Asn double-mutant Cyt*c*O). This conclusion is also consistent with results from other experimental studies,[55,65] results from the electrostatic calculations presented in Table 1, and results obtained earlier for a residue equivalent to Cys139 in the *P. denitrificans* Cyt*c*O.[59]

The 30% rapid proton uptake in the Asn139Cys/Asp132Asn double-mutant Cyt*c*O could be explained by a 30% deprotonated fraction (i.e., negatively charged) Cys139 or, perhaps more likely, in terms of a 30−70% equilibrium of two configurations of the Cys139 side chain such that in one state the D pathway would be open ($\tau \cong 250\ \mu s$) while in the other it would be closed [$\tau \cong 330$ ms (see above and ref 40)]. This conclusion is also supported by the results from the MD simulations, which show that the Cys139 and Asn121 side chains explore two conformations in both the Asn139Cys single mutant and the Asn139Cys/Asp132Asn double mutant, which would indicate that Cys139 may facilitate proton uptake also in the absence of Asp132.

It is also possible that the Asp132Asn mutation influences the protonation state of surrounding residues. One such candidate is His26, which is in close contact with the side chain carboxylate of Asp132. A strong hydrogen bond between (ionized) His26 and Asp132 is formed in the MD simulations of wild-type Cyt*c*O. Upon mutation to an Asn at position 132, our simulations suggest that the interaction between the residues becomes weaker and the distance between the side chains increases, which may lead to deprotonation of His26. This is also supported by the PROPKA method, which suggests that the pK_a of His26 is ~6 in the wild type and Asn139Cys mutant but decreases to ~3 in the Asn139Cys/Asp132Asn double mutant. The results from the MCCE method were not conclusive in this case. The protonation states predicted for Asp132 and His26 were very sensitive to the choice of snapshot from the MD simulation, often ranging from fully protonated to deprotonated at pH 7. This result is consistent with the observation that these residues sample a much larger number of conformations in the MD simulations than the more confined residues such as Glu286.

The conclusions outlined above would suggest that the effect of the Asn139Cys single mutation on the p$K_{a,PF}$ of Glu286 is not due to introduction of negative charge at position 139. In other words, the similarity between the p$K_{a,PF}$ effects observed with the Asn139Asp and Asn139Cys mutant Cyt*c*Os (where in both cases the Glu286 p$K_{a,PF}$ is increased compared to that of the wild-type Cyt*c*O) would be due to structural alterations and not due to introduction of charge at position 139. In this context, we note that charge−charge interactions must always be taken into account and a negative charge at position 139 would certainly result in an increase in the Glu286 p$K_{a,PF}$, even though different magnitudes have been calculated ranging from insignificant[59] to significant.[66] More recent data indicate that the position of the Asp139 side chain may be crucial for the charge−charge interactions with Glu286,[39] which would explain the different p$K_{a,PF}$ values observed with the Asn139Asp and Asn139Asp/Asp132Asn mutant Cyt*c*Os.[61] Nevertheless, the data from this work suggest that the structural effects are more dominant than the charge−charge interactions.

The results from the MD simulations indicate that the Glu286 side chain does not move upon replacement of Asn139 with Cys (not shown). However, as already indicated above, results from structural studies of the Asn131Asp mutant Cyt*c*O from *P. denitrificans* (corresponds to Asn139Asp in the *R. sphaeroides* Cyt*c*O)[41] and FTIR experiments[32] suggest that the side chain position and hydrogen bonding pattern of Glu278 (Glu286 in *R. sphaeroides* Cyt*c*O) may be modified upon modification of residue 139. Even though these structural changes are presumably relatively small, they may result in a change in the equilibrium constant between the two positions of Glu286 (see above). Because the free energy difference for the two positions (one of which is only transiently populated during the proton transfer) determines the apparent p$K_{a,PF}$, this value could be altered in the mutant Cyt*c*Os, which is proposed to result in uncoupling of the proton pump.[21,27,36,41,59] Alternatively, it has been proposed that structural changes around position 139 may result in slowed reprotonation of Glu286, which would also result in uncoupling of the proton pump.[29,40] However, irrespective of the assignment of pK_{aPF}, the experimentally observed proton-transfer rate at pH <9 is not slower, and at pH >9, it is faster with the Asn139Cys mutant Cyt*c*O than with the wild-type Cyt*c*O (Figure 3). Even though at pH <9 the transfer of a proton from solution to Glu286 is not rate-limiting for the overall proton transfer to the catalytic site,[24] the acceleration in the observed proton transfer at high pH in the Asn139Cys mutant Cyt*c*O indicates that proton transfer through the D pathway, via Cys139, to Glu286 is not slowed in the mutant Cyt*c*O. Instead, the most plausible explanation is that the amino acid replacement does alter the structure around Glu286, which results in impaired proton pumping, also reflected as a change in the Glu286 p$K_{a,PF}$.

AUTHOR INFORMATION

Corresponding Author

*E-mail: peterb@dbb.su.se. Fax: +46-8-153679. Phone: +46 70 609 2642.

Notes

The authors declare no competing financial interest.

ABBREVIATIONS

Cyt*c*O, cytochrome *c* oxidase; *n* side, negative side of the membrane; *p* side, positive side of the membrane; DDM, *n*-dodecyl β-D-maltoside; PDB, Protein Data Bank.

ADDITIONAL NOTE

[a]If not otherwise indicated, amino acid residues are numbered according to the *R. sphaeroides* Cyt*c*O sequence and the residues are found in subunit I.

REFERENCES

(1) Hosler, J. P., Ferguson-Miller, S., and Mills, D. A. (2006) Energy transduction: Proton transfer through the respiratory complexes. *Annu. Rev. Biochem. 75*, 165−187.

(2) Yoshikawa, S., Muramoto, K., Shinzawa-Itoh, K., Aoyama, H., Tsukihara, T., Shimokata, K., Katayama, Y., and Shimada, H. (2006) Proton pumping mechanism of bovine heart cytochrome c oxidase. *Biochim. Biophys. Acta 1757*, 1110−1116.

(3) Wikström, M., and Verkhovsky, M. I. (2006) Towards the mechanism of proton pumping by the haem-copper oxidases. *Biochim. Biophys. Acta 1757*, 1047−1051.

(4) Namslauer, A., and Brzezinski, P. (2004) Structural elements involved in electron-coupled proton transfer in cytochrome c oxidase. *FEBS Lett. 567*, 103−110.

(5) Brzezinski, P., and Gennis, R. B. (2008) Cytochrome c oxidase: Exciting progress and remaining mysteries. *J. Bioenerg. Biomembr. 40*, 521−531.

(6) Brzezinski, P., and Ädelroth, P. (2006) Design principles of proton-pumping haem-copper oxidases. *Curr. Opin. Struct. Biol. 16*, 465−472.

(7) Richter, O. M. H., and Ludwig, B. (2009) Electron transfer and energy transduction in the terminal part of the respiratory chain: Lessons from bacterial model systems. *Biochim. Biophys. Acta 1787*, 626−634.

(8) Belevich, I., and Verkhovsky, M. I. (2008) Molecular mechanism of proton translocation by cytochrome c oxidase. *Antioxid. Redox Signaling 10*, 1−29.

(9) Ferguson-Miller, S., Hiser, C., and Liu, J. (2012) Gating and regulation of the cytochrome c oxidase proton pump. *Biochim. Biophys. Acta 1817*, 489−494.

(10) Qin, L., Hiser, C., Mulichak, A., Garavito, R. M., and Ferguson-Miller, S. (2006) Identification of conserved lipid/detergent-binding sites in a high-resolution structure of the membrane protein cytochrome c oxidase. *Proc. Natl. Acad. Sci. U.S.A. 103*, 16117−16122.

(11) Svensson-Ek, M., Abramson, J., Larsson, G., Törnroth, S., Brzezinski, P., and Iwata, S. (2002) The X-ray Crystal Structures of Wild-Type and EQ(I-286) Mutant Cytochrome *c* Oxidases from *Rhodobacter sphaeroides*. *J. Mol. Biol. 321*, 329−339.

(12) Smirnova, I. A., Ädelroth, P., Gennis, R. B., and Brzezinski, P. (1999) Aspartate-132 in cytochrome *c* oxidase from *Rhodobacter sphaeroides* is involved in a two-step proton transfer during oxo-ferryl formation. *Biochemistry 38*, 6826−6833.

(13) Gorbikova, E. A., Belevich, N. P., Wikström, M., and Verkhovsky, M. I. (2007) Time-resolved ATR-FTIR spectroscopy of the oxygen reaction in the D124N mutant of cytochrome c oxidase from *Paracoccus denitrificans*. *Biochemistry 46*, 13141−13148.

(14) Kaila, V. R. I., Verkhovsky, M. I., Hummer, G., and Wikström, M. (2008) Glutamic acid 242 is a valve in the proton pump of cytochrome c oxidase. *Proc. Natl. Acad. Sci. U.S.A. 105*, 6255−6259.

(15) Popovic, D. M., and Stuchebrukhov, A. A. (2006) Two conformational states of Glu242 and pKas in bovine cytochrome c oxidase. *Photochem. Photobiol. Sci. 5*, 611−620.

(16) Ädelroth, P., Karpefors, M., Gilderson, G., Tomson, F. L., Gennis, R. B., and Brzezinski, P. (2000) Proton transfer from glutamate 286 determines the transition rates between oxygen intermediates in cytochrome c oxidase. *Biochim. Biophys. Acta 1459*, 533−539.

(17) Pomès, R., Hummer, G., and Wikström, M. (1998) Structure and dynamics of a proton shuttle in cytochrome c oxidase. *Biochim. Biophys. Acta 1365*, 255−260.

(18) Qin, L., Liu, J., Mills, D. A., Proshlyakov, D. A., Hiser, C., and Ferguson-Miller, S. (2009) Redox-dependent conformational changes in cytochrome c oxidase suggest a gating mechanism for proton uptake. *Biochemistry 48*, 5121−5130.

(19) Busenlehner, L. S., Brändén, G., Namslauer, I., Brzezinski, P., and Armstrong, R. N. (2008) Structural elements involved in proton translocation by cytochrome c oxidase as revealed by backbone amide hydrogen-deuterium exchange of the E286H mutant. *Biochemistry 47*, 73−83.

(20) Pisliakov, A. V., Sharma, P. K., Chu, Z. T., Haranczyk, M., and Warshel, A. (2008) Electrostatic basis for the unidirectionality of the primary proton transfer in cytochrome c oxidase. *Proc. Natl. Acad. Sci. U.S.A. 105*, 7726−7731.

(21) Chakrabarty, S., Namslauer, I., Brzezinski, P., and Warshel, A. (2011) Exploration of the cytochrome c oxidase pathway puzzle and examination of the origin of elusive mutational effects. *Biochim. Biophys. Acta 1807*, 413−426.

(22) Riistama, S., Hummer, G., Puustinen, A., Dyer, R. B., Woodruff, W. H., and Wikström, M. (1997) Bound water in the proton translocation mechanism of the haem-copper oxidases. *FEBS Lett. 414*, 275−280.

(23) Hofacker, I., and Schulten, K. (1998) Oxygen and proton pathways in cytochrome c oxidase. *Proteins 30*, 100−107.

(24) Peng, Y., and Voth, G. A. (2012) Expanding the view of proton pumping in cytochrome c oxidase through computer simulation. *Biochim. Biophys. Acta 1817*, 518−525.

(25) Yang, S., and Cui, Q. (2011) Glu-286 rotation and water wire reorientation are unlikely the gating elements for proton pumping in cytochrome c oxidase. *Biophys. J. 101*, 61−69.

(26) Kaila, V. R. I., Verkhovsky, M. I., and Wikström, M. (2010) Proton-coupled electron transfer in cytochrome oxidase. *Chem. Rev. 110*, 7062−7081.

(27) Brzezinski, P., and Johansson, A. L. (2010) Variable proton-pumping stoichiometry in structural variants of cytochrome c oxidase. *Biochim. Biophys. Acta 1797*, 710−723.

(28) Namslauer, A., Aagaard, A., Katsonouri, A., and Brzezinski, P. (2003) Intramolecular proton-transfer reactions in a membrane-bound proton pump: The effect of pH on the peroxy to ferryl transition in cytochrome c oxidase. *Biochemsitry 42*, 1488−1498.

(29) Wikström, M., and Verkhovsky, M. I. (2011) The D-channel of cytochrome oxidase: An alternative view. *Biochim. Biophys. Acta 1807*, 1273−1278.

(30) Salomonsson, L., Brändén, G., and Brzezinski, P. (2008) Deuterium isotope effect of proton pumping in cytochrome c oxidase. *Biochim. Biophys. Acta 1777*, 343−350.

(31) Pfitzner, U., Hoffmeier, K., Harrenga, A., Kannt, A., Michel, H., Bamberg, E., Richter, O. M. H., and Ludwig, B. (2000) Tracing the D-pathway in reconstituted site-directed mutants of cytochrome c oxidase from *Paracoccus denitrificans*. *Biochemistry 39*, 6756−6762.

(32) Vakkasoglu, A. S., Morgan, J. E., Han, D., Pawate, A. S., and Gennis, R. B. (2006) Mutations which decouple the proton pump of the cytochrome c oxidase from *Rhodobacter sphaeroides* perturb the environment of glutamate 286. *FEBS Lett. 580*, 4613−4617.

(33) Zhu, J., Han, H., Pawate, A., and Gennis, R. B. (2010) Decoupling mutations in the D-channel of the aa_3-type cytochrome *c* oxidase from *Rhodobacter sphaeroides* suggest that a continuous hydrogen-bonded chain of waters is essential for proton pumping. *Biochemistry 49*, 4476−4482.

(34) Namslauer, A., Pawate, A. S., Gennis, R. B., and Brzezinski, P. (2003) Redox-coupled proton translocation in biological systems: Proton shuttling in cytochrome c oxidase. *Proc. Natl. Acad. Sci. U.S.A. 100*, 15543−15547.

(35) Lepp, H., Salomonsson, L., Zhu, J. P., Gennis, R. B., and Brzezinski, P. (2008) Impaired proton pumping in cytochrome c oxidase upon structural alteration of the D pathway. *Biochim. Biophys. Acta 1777*, 897−903.

(36) Johansson, A. L., Chakrabarty, S., Berthold, C. L., Högbom, M., Warshel, A., and Brzezinski, P. (2011) Proton-transport mechanisms in cytochrome c oxidase revealed by studies of kinetic isotope effects. *Biochim. Biophys. Acta 1807*, 1083−1094.

(37) Olsson, M. H., and Warshel, A. (2006) Monte Carlo simulations of proton pumps: On the working principles of the biological valve that controls proton pumping in cytochrome c oxidase. *Proc. Natl. Acad. Sci. U.S.A. 103*, 6500−6505.

(38) Xu, J., and Voth, G. A. (2006) Free energy profiles for H^+ conduction in the D-pathway of cytochrome c oxidase: A study of the wild type and N98D mutant enzymes. *Biochim. Biophys. Acta 1757*, 852−859.

(39) Henry, R. M., Caplan, D., Fadda, E., and Pomès, R. (2011) Molecular basis of proton uptake in single and double mutants of cytochrome c oxidase. *J. Phys.: Condens. Matter 23*, 234102.
(40) Henry, R. M., Yu, C. H., Rodinger, T., and Pomès, R. (2009) Functional Hydration and Conformational Gating of Proton Uptake in Cytochrome c Oxidase. *J. Mol. Biol. 387*, 1165−1185.
(41) Duerr, K. L., Koepke, J., Hellwig, P., Mueller, H., Angerer, H., Peng, G., Olkhova, E., Richter, O. M. H., Ludwig, B., and Michel, H. (2008) A D-Pathway Mutation Decouples the *Paracoccus denitrificans* Cytochrome c Oxidase by Altering the Side-Chain Orientation of a Distant Conserved Glutamate. *J. Mol. Biol. 384*, 865−877.
(42) Mitchell, D. M., and Gennis, R. B. (1995) Rapid purification of wildtype and mutant cytochrome c oxidase from *Rhodobacter sphaeroides* by Ni^{2+}-NTA affinity chromatography. *FEBS Lett. 368*, 148−150.
(43) Zhen, Y., Qian, J., Follmann, K., Hosler, J., Hayward, T., Nilsson, T., Dahn, M., Hilmi, Y., Hamer, A., Hosler, J., and Ferguson-Miller, S. (1998) Overexpression and purification of cytochrome coxidase from *Rhodobacter sphaeroides*. Protein Expression and Purification. *Protein Expression Purif. 13*, 326−336.
(44) Hess, B., Kutzner, C., van der Spoel, D., and Lindahl, E. (2008) GROMACS 4: Algorithms for highly efficient, load-balanced, and scalable molecular simulation. *J. Chem. Theory Comput. 4*, 435−447.
(45) Jorgensen, W. L., Maxwell, D. S., and TiradoRives, J. (1996) Development and testing of the OPLS all-atom force field on conformational energetics and properties of organic liquids. *J. Am. Chem. Soc. 118*, 11225−11236.
(46) Berger, O., Edholm, O., and Jahnig, F. (1997) Molecular dynamics simulations of a fluid bilayer of dipalmitoylphosphatidylcholine at full hydration, constant pressure, and constant temperature. *Biophys. J. 72*, 2002−2013.
(47) Jorgensen, W. L., Chandrasekhar, J., Madura, J. D., Impey, R. W., and Klein, M. L. (1983) Comparison of Simple Potential Functions for Simulating Liquid Water. *J. Chem. Phys. 79*, 926−935.
(48) Marelius, J., Kolmodin, K., Feierberg, I., and Åqvist, J. (1998) Q: A molecular dynamics program for free energy calculations and empirical valence bond simulations in biomolecular systems. *J. Mol. Graphics Modell. 16*, 213−225.
(49) Ryckaert, J. P., Ciccotti, G., and Berendsen, H. J. C. (1977) Numerical-Integration of Cartesian Equations of Motion of a System with Constraints: Molecular-Dynamics of N-Alkanes. *J. Comput. Phys. 23*, 327−341.
(50) King, G., and Warshel, A. (1989) A Surface Constrained All-Atom Solvent Model for Effective Simulations of Polar Solutions. *J. Chem. Phys. 91*, 3647−3661.
(51) Lee, F. S., and Warshel, A. (1992) A Local Reaction Field Method for Fast Evaluation of Long-Range Electrostatic Interactions in Molecular Simulations. *J. Chem. Phys. 97*, 3100−3107.
(52) Olsson, M. H. M., Sondergaard, C. R., Rostkowski, M., and Jensen, J. H. (2011) PROPKA3: Consistent Treatment of Internal and Surface Residues in Empirical pK_a Predictions. *J. Chem. Theory Comput. 7*, 525−537.
(53) Alexov, E. G., and Gunner, M. R. (1997) Incorporating protein conformational flexibility into the calculation of pH-dependent protein properties. *Biophys. J. 72*, 2075−2093.
(54) Nicholls, A., and Honig, B. (1991) A Rapid Finite-Difference Algorithm, Utilizing Successive Over-Relaxation to Solve the Poisson-Boltzmann Equation. *J. Comput. Chem. 12*, 435−445.
(55) Varanasi, L., and Hosler, J. (2011) Alternative initial proton acceptors for the D pathway of *Rhodobacter sphaeroides* cytochrome c oxidase. *Biochemistry 50*, 2820−2828.
(56) Lübben, M., Prutsch, A., Mamat, B., and Gerwert, K. (1999) Electron transfer induces side-chain conformational changes of glutamate-286 from cytochrome bo_3. *Biochemistry 38*, 2048−2056.
(57) Ghosh, N., Xavier, P. R., Gunner, M. R., and Cui, Q. (2009) Microscopic pK_a analysis of Glu286 in cytochrome c oxidase (*Rhodobacter sphaeroides*): Toward a calibrated molecular model. *Biochemistry 48*, 2468−2485.
(58) Popovic, D. M., Leontyev, I. V., Beech, D. G., and Stuchebrukhov, A. A. (2010) Similarity of cytochrome c oxidases in different organisms. *Proteins: Struct., Funct., Bioinf. 78*, 2691−2698.
(59) Olkhova, E., Helms, V., and Michel, H. (2005) Titration behavior of residues at the entrance of the D-pathway of cytochrome c oxidase from *Paracoccus denitrificans* investigated by continuum electrostatic calculations. *Biophys. J. 89*, 2324−2331.
(60) Fetter, J. R., Qian, J., Shapleigh, J., Thomas, J. W., García-Horsman, A., Schmidt, E., Hosler, J., Babcock, G. T., Gennis, R. B., and Ferguson-Miller, S. (1995) Possible proton relay pathways in cytochrome c oxidase. *Proc. Natl. Acad. Sci. U.S.A. 92*, 1604−1608.
(61) Brändén, G., Pawate, A. S., Gennis, R. B., and Brzezinski, P. (2006) Controlled uncoupling and recoupling of proton pumping in cytochrome *c* oxidase. *Proc. Natl. Acad. Sci. U.S.A. 103*, 317−322.
(62) García-Horsman, J. A., Puustinen, A., Gennis, R. B., and Wikström, M. (1995) Proton transfer in cytochrome bo_3 ubiquinol oxidase of *Escherichia coli*: Second-site mutations in subunit I that restore proton pumping in the mutant Asp135→Asn. *Biochemistry 34*, 4428−4433.
(63) Paddock, M. L., Ädelroth, P., Feher, G., Okamura, M. Y., and Beatty, J. T. (2002) Determination of proton transfer rates by chemical rescue: Application to bacterial reaction centers. *Biochemistry 41*, 14716−14725.
(64) Song, Y., Michonova-Alexova, E., and Gunner, M. R. (2006) Calculated proton uptake on anaerobic reduction of cytochrome c oxidase: Is the reaction electroneutral? *Biochemistry 45*, 7959−7975.
(65) Varanasi, L., and Hosler, J. P. (2012) Subunit III-depleted cytochrome c oxidase provides insight into the process of proton uptake by proteins. *Biochim. Biophys. Acta 1817*, 545−551.
(66) Fadda, E., Yu, C. H., and Pomès, R. (2008) Electrostatic control of proton pumping in cytochrome c oxidase. *Biochim. Biophys. Acta 1777*, 277−284.
(67) DeLano, W. L. (2002) *The PyMOL Molecular Graphics System*, DeLano Scientific, Palo Alto, CA.